Journal of Physics:
Conference Series

PURPOSE-LED PUBLISHING™

PAPER • OPEN ACCESS

Design and characterization of small-sized Kiel-type shielded probes

To cite this article: W. Al Hroub *et al* 2026 *J. Phys.: Conf. Ser.* **3271** 012024

View the article online for updates and enhancements.

You may also like

- Polarization- and angle-insensitive plasmon-induced transparency in four-fold symmetric graphene metamaterials
Ziyu Wang and Weijie Shi
- Extremely bending-resistant and compression-insensitive flexible circuits enabled by real-time crack healing via spontaneous interfacial wetting
Sheng Li, Liang Wang, Xiaoliang Chen et al.
- Ultra-wideband terahertz metamaterial absorber with polarization insensitivity and broad incidence angle absorption
Yanpeng Zhang, Xuehong Sun, Zhanxiong Li et al.

SmarAct | group

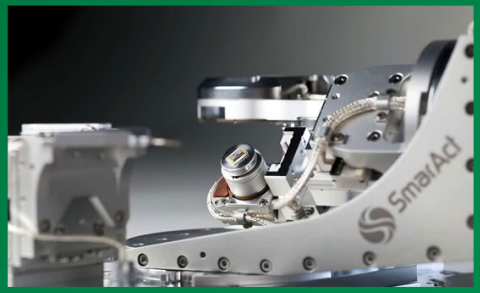
webinar

More details and registration

One sample, many dimensions: prospects for multimodal nanoscale characterization

Explore how precise sample manipulation enables complementary nanoscale techniques to work together on one sample

Live at 2 p.m. GMT/3 p.m. CET,
12 November 2026



This content was downloaded from IP address 144.122.201.61 on 16/11/2026 at 16:54

Journal of Physics: Conference Series **3271** (2026) 012024 doi:10.1088/1742-6596/3271/1/012024

Design and characterization of small-sized Kiel-type shielded probes

W. Al Hroub[1], Z. Anwar[1], M. Yazdanpanah[1], B. Doğan[2] and M. Perçin[1]

[1]Department of Aerospace Engineering, Middle East Technical University, Ankara, Türkiye
[2]METU Center for Wind Energy Research (RÜZGEM), Ankara, Türkiye

E-mail: wesam.hroub@metu.edu.tr

Abstract. This study focuses on the optimization and parameterization of an approximately 3 mm diameter Kiel-type (shielded) probe for accurate total pressure measurements to meet an angular insensitivity range of ±45° operating under subsonic flow conditions. The work is motivated by the need for compact, angularly insensitive probes in turbomachinery, where conventional pitot tubes suffer severe accuracy losses at large incidence angles. A literature-based design analysis was combined with stringent manufacturing constraints (e.g., minimum printable wall thickness) to establish a parametric framework for probe geometry. An existing industrial design was analysed for baseline comparison. Using Computational Fluid Dynamics (CFD) simulations with the Reynolds Stress Model (RSM), geometric parameters were studied and optimised to adapt the probe for miniature applications while minimising angular sensitivity. The resulting angular insensitivity obtained from numerical simulations for the optimised probe (Proposed Probe 3) is ±46°. The improved design was manufactured and tested, confirming its reliable performance over a wide angular range with an angular insensitivity value of approximately ±50.5°. This work demonstrates the feasibility of miniaturising Kiel probes while preserving aerodynamic efficiency, and establishes a parametric methodology for tailoring probe geometries to confined applications such as turbomachinery.

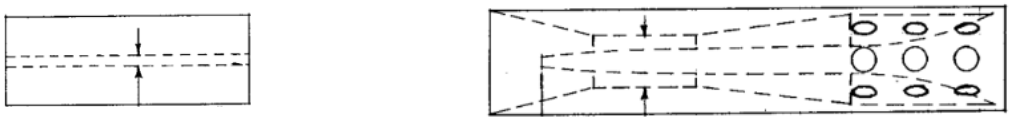
1 Introduction

In aerodynamic experiments and real-life applications, accurate total pressure measurement is crucial, particularly when flow incidence angles are large and flow direction varies. Pressure measurement probes must maintain precision despite these challenges. Among various designs, Kiel probes have proven particularly effective due to their ability to compensate for flow angularity by straightening the streamlines as they enter the probe, increasing the accuracy of the measurement compared to conventional pitot tubes [1]. NASA Technical Note 3641 [2] compared conventional pitot tubes with shielded Kiel-type probes (figure 1). The study showed that the conventional pitot probe provides accurate pressure readings only at small incidence angles, since misalignment with the freestream leads to significant errors. In contrast, the Kiel-type probe employs a shielding shroud that guides the incoming flow, resulting in an increased range of angular insensitivity. This characteristic makes Kiel probes more suitable for applications where flow direction varies significantly. In this study, the angular insensitivity range is defined as the incidence angle interval over which the probe measures total pressure within ±1% error

Content from this work may be used under the terms of the Creative Commons Attribution 4.0 licence. Any further distribution of this work must maintain attribution to the author(s) and the title of the work, journal citation and DOI.
Published under licence by IOP Publishing Ltd

relative to the reference zero-angle value. It is important to mention that the functionality of Kiel probes is based on limited studies that are generally from the 20th century, since recent studies about their aerodynamic behaviour are limited.

This study focuses on developing a miniature Kiel probe with a diameter of approximately 3 mm capable of maintaining accuracy across a $\pm 45^\circ$ angular range while meeting modern production constraints.



(a) (b)

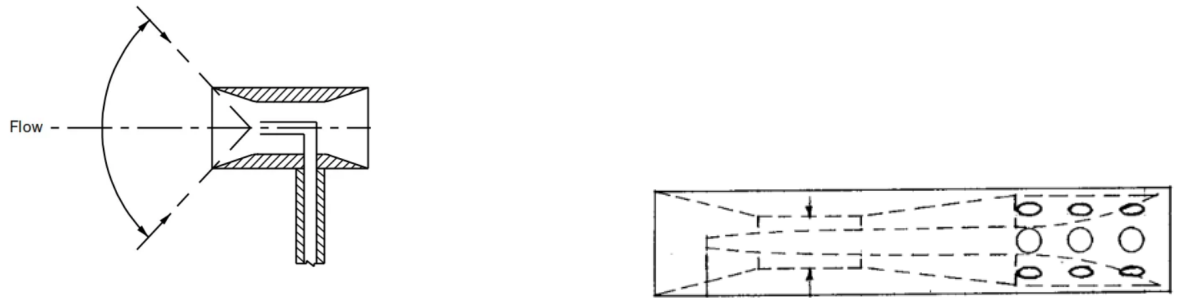
Figure 1: (a) Conventional pitot probe. (b) Kiel-type shielded probe [2].

Several key geometric parameters influence the performance of a Kiel probe. The axial spacing ratio (a/D_1), defined as the distance between the probe tip and the shield lip relative to the outer shield diameter D_1, directly affects the consistency and accuracy of pressure readings. Kiel's original tests [1] identified an optimal value of 0.50, while subsequent studies reported that a reduced value of 0.456 can maintain accuracy with reduced sensitivity variation [3]. The diameter ratios are also critical. Here, d denotes the diameter at the inner edge of the sensing passage, D the diameter at the outer edge of the inner probe, and D_2 is the diameter of the throat of the probe. The impact opening ratio (d/D) reflects the relative size of the inner passage, while the throat-to-shield ratio (D_2/D_1) relates the throat of the probe to the shield diameter. Both ratios strongly impact angular insensitivity and flow alignment [2], though they are constrained by manufacturing limitations, particularly the minimum printable wall thickness in additive manufacturing. Other crucial parameters include the entrance angle (β), where smoothly contoured entries and sharper inlet edges have been shown to extend the angular range and improve performance [3]. Finally, the vent-to-inlet area ratio (A_v/A_o) influences insensitivity, particularly at low Mach numbers, although increases beyond a ratio of 1.5 yield diminishing benefits [2].

There are two main types of Kiel probes: open shielded and closed shielded designs (figure 2). The open shielded Kiel probe incorporates an L-shaped or open shroud, which provides superior insensitivity to flow angularity; on the other hand, the closed shielded Kiel probe employs a straight tubular shroud with vent holes and is sometimes preferred when a rake or grid of probes is required for multi-point measurements [4]. In this study, the horizontal closed-shield configuration was adopted, since it offers practical advantages in multi-probe arrangements and, importantly, provides increased structural robustness against vibrations during experiments — a limitation that has been highlighted previously in the literature for spindle-type or open configurations [5].

Miniature probe design introduces additional fabrication challenges: wall thickness constraints from additive manufacturing restrict geometric optimisations, particularly for diameter ratios. While simulations suggest curved internal profiles could help, the design achieves target performance without this feature. Vent geometry modifications were necessary, as sharp circular vents induced undesirable recirculation at high angles; this was mitigated by implementing an aerodynamically optimised profile.

The aim of this study is to design and fabricate a miniature Kiel probe using 3D metal printing technology that is optimised for accurate performance in subsonic flow conditions. A



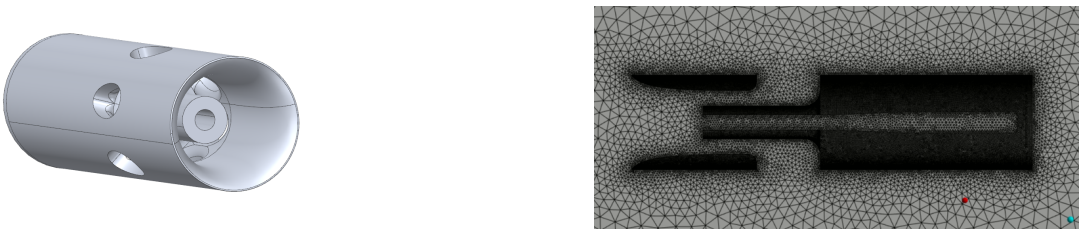
(a) (b)

Figure 2: (a) Open shielded Kiel probe [6]. (b) Closed shielded Kiel probe [2].

comparative investigation was conducted between a pre-existing Kiel probe and a newly proposed configuration tailored for compact applications. Both geometries were analysed using CFD simulations with the RSM at Mach 0.083 for the pre-existing model, to match the available experimental data obtained using the jet calibrator, and Mach 0.28 for the other probes, aligning with literature standards. Experimental validation was carried out using a jet calibrator operating at a low Mach number of 0.083 due to equipment limitations. However, this does not compromise the results, as the existing literature confirms that the accuracy of shielded probes, such as Kiel probes, increases as Mach number decreases [2]. The optimised design was then fabricated and tested experimentally to assess its performance under the defined constraints.

2 Methods

The Kiel probe geometry is characterised by several critical parameters that determine its performance. The pre-existing design taken as baseline is referred to as the Conventional Probe (figure 3). It follows established designs with sharp elliptical vent holes. The optimisation process followed in this study, starting from the experimentally tested baseline design, is an iterative CFD-driven optimisation described in the block diagram (figure 4). The probes were manufactured using Direct Metal Laser Sintering (DMLS) technology with stainless steel, which allows precise realisation of complex internal geometries while maintaining the required outer diameter specification. The manufacturing process particularly influenced the proposed design's vent geometry and wall thickness parameters.



(a) (b)

Figure 3: (a) 3D geometry of the Conventional Probe. (b) Computational mesh of the Conventional Probe.

First, an off-the-shelf Kiel probe was experimentally tested using the jet calibrator facility described at the end of this section. The same geometry was then simulated with CFD under a coarse mesh to establish a computational setup that reproduced experimental results reliably.

This validated setup was subsequently applied to candidate probe geometries. Literature-based designs were modified iteratively under two primary constraints: (i) an outer diameter limited to 3–3.5 mm, and (ii) a minimum manufacturable wall thickness of 0.35 mm dictated by DMLS printing. Each design was screened in CFD for angular insensitivity, followed by a manufacturability check; non-compliant geometries were either adapted or replaced by alternatives. Through this loop, three candidate probes were evaluated.

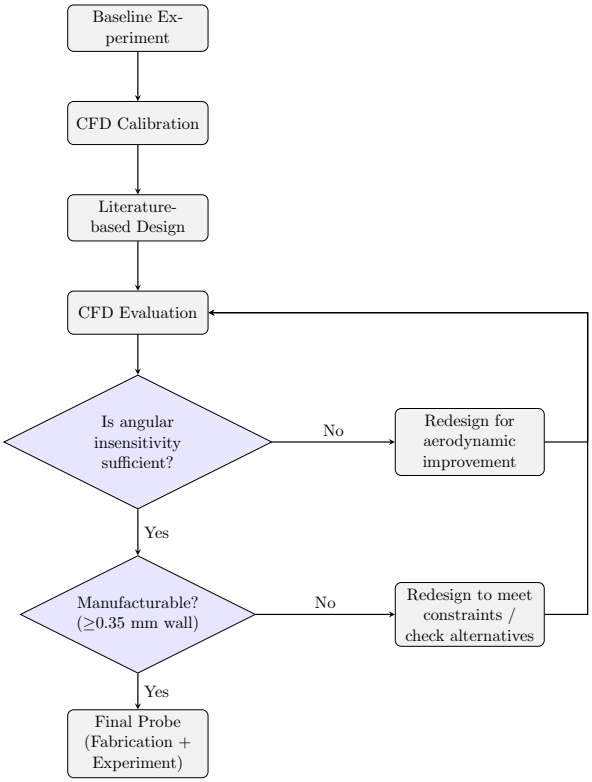
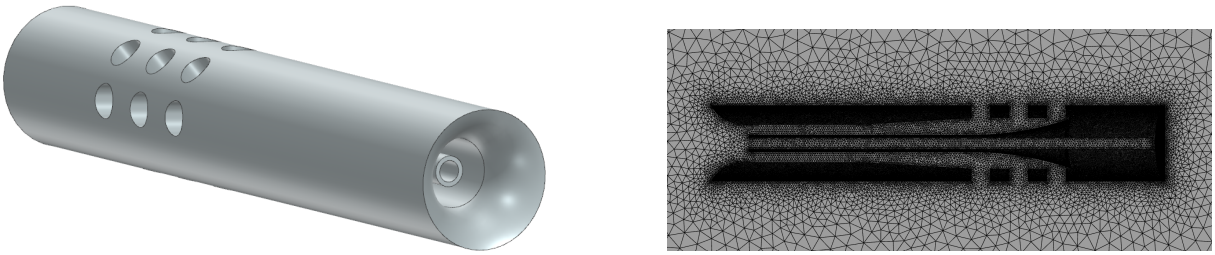


Figure 4: Flowchart of the CFD-driven optimisation and manufacturability loop for probe design.

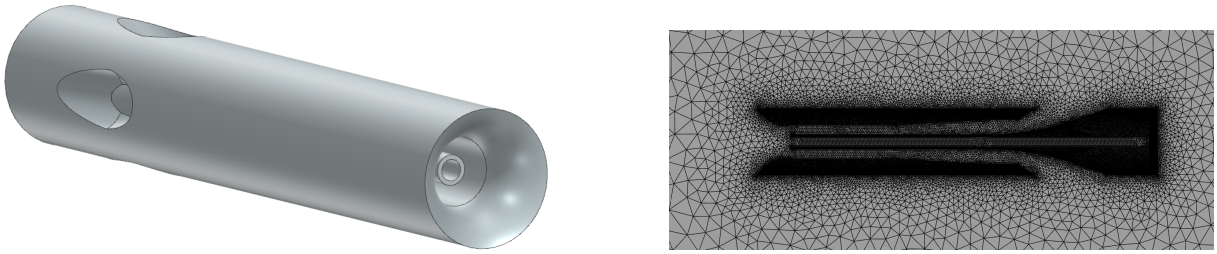
The first design, Proposed Probe 1 (figure 5), was adapted from literature. While it provided sufficient angular insensitivity in the CFD evaluation, the results (see section 3) revealed the presence of recirculation zones around the circular holes. This observation motivated a redesign to achieve improved aerodynamic performance by making the vent holes more aerodynamically favoured.



(a) (b)

Figure 5: (a) 3D geometry of Proposed Probe 1. (b) Computational mesh of Proposed Probe 1.

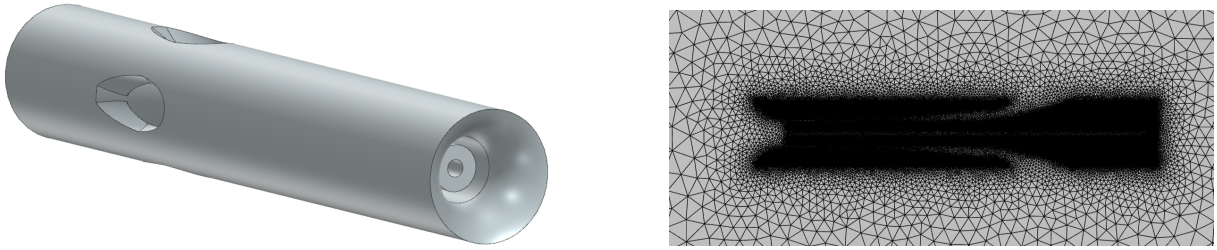
Improving the vent geometry to a more aerodynamically favourable shape resulted in Proposed Probe 2 (figure 6). This modification increased the range of angular insensitivity. However, the design failed to satisfy the manufacturability constraint for the inner probe, as the wall thickness was below the allowable limit. This limitation led to a subsequent redesign.



(a) (b)

Figure 6: (a) 3D geometry of Proposed Probe 2. (b) Computational mesh of Proposed Probe 2.

Meeting the manufacturability constraints while incorporating the enhanced aerodynamically preferred vent holes and passing the anticipated angular insensitivity range, Proposed Probe 3 (figure 7) was then fabricated and experimentally tested.



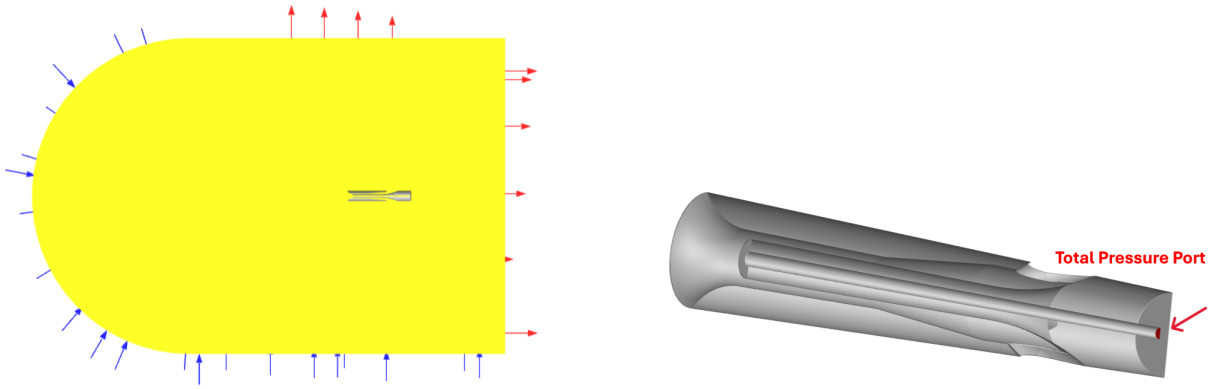
(a) (b)

Figure 7: (a) 3D geometry of Proposed Probe 3. (b) Computational mesh of Proposed Probe 3.

Numerical simulations were performed using ANSYS Fluent. A viscous, incompressible flow assumption was adopted, as the freestream Mach number of 0.28 falls within the incompressible regime and is consistent with standard literature test conditions. All simulations were conducted under steady-state conditions for each angle of attack, using the pressure-based solver. Convergence was typically achieved within 3000 iterations.

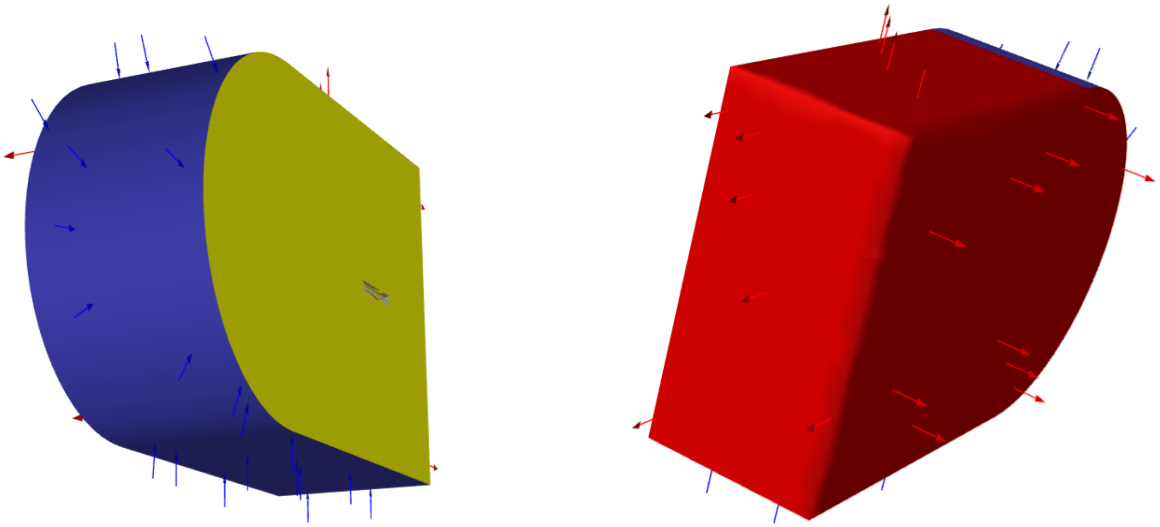
The governing equations consisted of the Reynolds-Averaged Navier–Stokes (RANS) equations — continuity and momentum — with turbulence closure provided by the Reynolds Stress Model (RSM). In particular, the linear pressure–strain variant of the RSM was used, which solves transport equations for all six Reynolds stress components together with a dissipation rate equation (7-equation form). This approach was selected for its ability to capture anisotropy, separation, and the expected strong streamline curvature in shielded probe flows [7]. The mathematical formulation of the RANS and RSM equations can be found in the ANSYS Fluent Theory Guide [8].

The computational domain (figures 8 and 9) consisted of a three-dimensional model of the probe cut in half, with a symmetry boundary applied along the mid-plane to reduce computational cost. The domain featured a rounded and flat lower boundary, with a velocity inlet which for the proposed probes assumed a magnitude of 95.27 $\mathrm{m\,s^{-1}}$, corresponding to



(a) (b)

Figure 8: (a) Domain shape and boundary conditions. (b) Probe geometry with pressure port location.



(a) (b)

Figure 9: (a) Velocity inlet boundary condition. (b) Pressure outlet boundary condition.

Mach 0.28, while for the experimentally tested baseline Conventional Probe a velocity magnitude of 28.14 $\mathrm{m\,s^{-1}}$, corresponding to Mach 0.083, was applied to match the experimental conditions, at $\rho = 1.225\ \mathrm{kg\,m^{-3}}$, $T = 288.16$ K, $\gamma = 1.4$, and $\mu = 1.789 \times 10^{-5}\ \mathrm{kg\,m^{-1}\,s^{-1}}$ with turbulence intensity of 5% and turbulence viscosity ratio of 10. The pressure outlet was set to ambient conditions, mimicking the open-jet test environment. Probe walls were treated as no-slip and adiabatic, and a pressure port boundary was defined to extract total pressure readings.

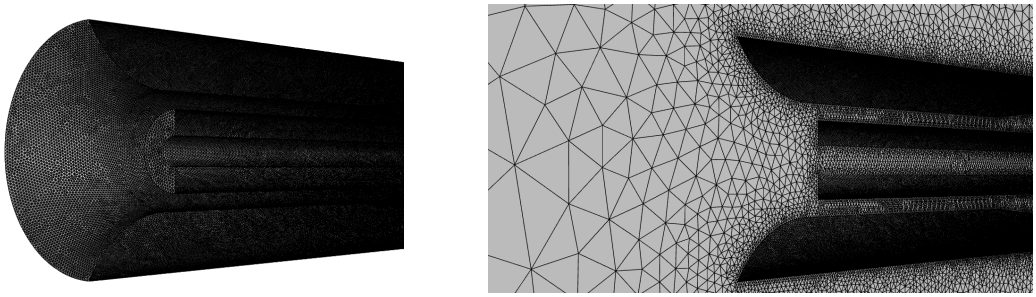
The mesh figures shown in the paper are sectional cuts of the full 3D domain for clarity. An axisymmetric simulation was not used, as the vent holes and internal geometry of the probe break rotational symmetry (in such a setup, the solver would artificially smear the vents into a continuous annular slot, misrepresenting the flow physics), requiring a full 3D treatment to capture the flow physics accurately.

Meshing followed an unstructured tetrahedral approach with local refinement about the

probe due to the presence of complex geometries such as vent holes and a curved inlet (figures 10 and 11). Explicit inflation layers along the probe walls were not applied, as the primary focus of this study was on total pressure recovery and angular insensitivity rather than wall shear stress resolution. This choice is not expected to significantly affect the results, since wall shear effects play only a secondary role compared to probe pressure response. Instead, mesh density was globally increased around the probe geometry to capture recirculation zones and streamline alignment. Mesh resolution was first calibrated against experimental data for the baseline probe to ensure agreement. For the proposed probes, comparatively finer meshes were used to improve aerodynamic fidelity. The mesh element counts of the Conventional Probe and Proposed Probe 3 are shown in table 1.

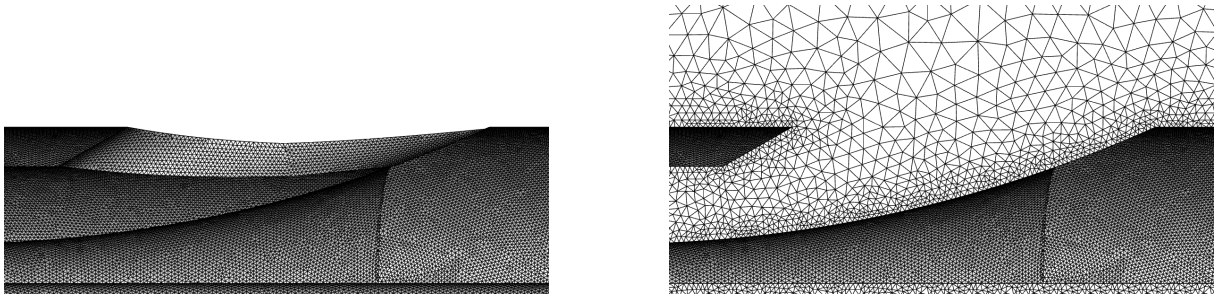
Table 1: Mesh element counts for different probe designs.

Probe Design	**Mesh Element Count**
Conventional Probe	1,323,516
Proposed Probe 3	3,252,168



(a) (b)

Figure 10: (a) Mesh around the probe surface near the flow inlet. (b) Mesh on the symmetry plane near the probe wall.



(a) (b)

Figure 11: (a) Mesh detail around the probe surface and diffuser region. (b) Mesh detail at the symmetry plane near probe walls.

Jet flow calibration measurements were conducted using RÜZGEM's specialised test facility (figure 12) [9]. The jet calibrator was operated using an in-house LabVIEW code with a PID

controller, ensuring a uniform and constant outlet velocity. The probe was mounted on a rigid arm with precise angular control via a calibrated rotary device. A subsonic jet nozzle (Mach 0.083) positioned below the probe created a stable flow field, with total pressure recorded at discrete angle increments. This configuration enabled direct performance comparison between conventional and proposed probes under identical flow conditions, with particular attention to their $\pm 45^\circ$ angular range specification.

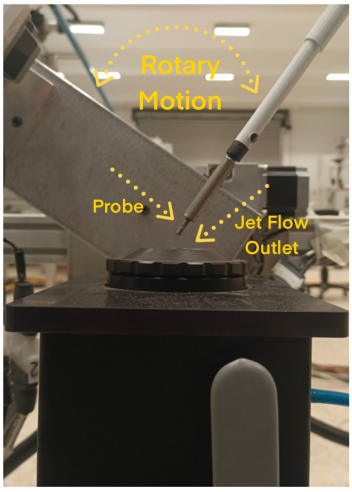


Figure 12: Jet calibrator at RÜZGEM.

3 Results and discussion

3.1 Proposed Probe 1

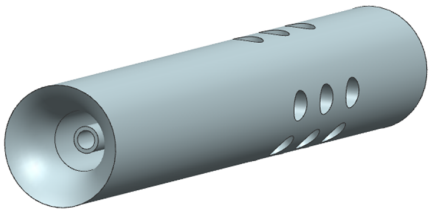


Figure 13: Proposed Probe 1.

The first design (figure 13) obeys all the considerations from the literature study, tailored to the miniature size. To facilitate the ratio of outer and inner diameters from the literature study and the manufacturing constraints, it was suggested to design a probe such that it used an already manufactured inner probe of minimum thickness. The remaining parameters were consistent with the literature study. CFD simulations showed impressive results with an angular range of approximately $\pm 53^\circ$. However, a detailed examination of cross sections of the probe showed some aerodynamic inefficiencies, such as recirculation and inward flow from vent holes at higher angles of attack (figure 14).

It was hypothesised that aligning the vent holes with the freestream would enhance pressure recovery and reduce recirculation. This approach optimises the design for the least amount of recirculation by improving the vent holes. The optimisation was performed for Proposed Probe 2.

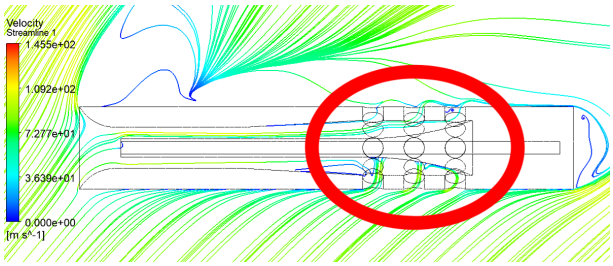


Figure 14: Streamlines overlaid on velocity magnitude contours, indicating flow recirculation in the vent passages.

3.2 Proposed Probe 2



(a) (b)

Figure 15: (a) Geometry of Proposed Probe 2 showing the modified internal structure. (b) Updated vent and diffuser configuration designed to reduce recirculation and enhance aerodynamic performance.

The CFD analysis of Proposed Probe 2 (figure 15) showed an increase in the angular range with the optimised design, reaching approximately $\pm 57°$. This supported the hypothesis that the design of vent holes affects the aerodynamic efficiency of the whole probe. The vent and diffuser were designed to reduce recirculation and increase probe efficiency. The results (figure 16) show reduced recirculation and inward flow at the aerodynamically optimised vent. However, it was found to be more feasible to design the probe using additive manufacturing as a whole instead of attaching an already manufactured inner probe of smaller thickness, which led to the design of Proposed Probe 3, where manufacturing constraints and refined vent holes are included.

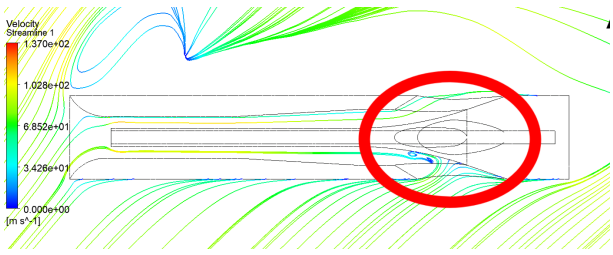
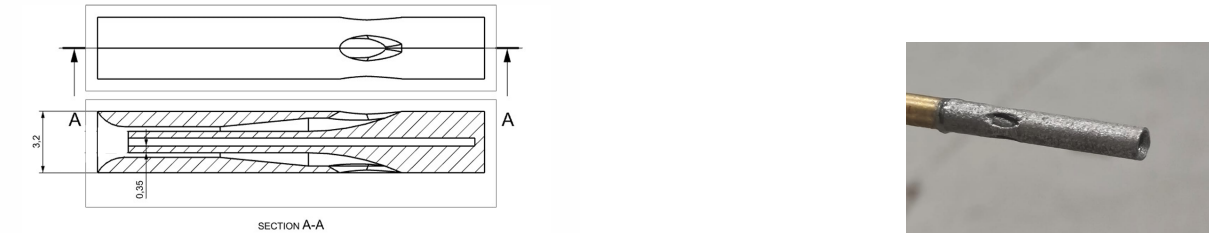


Figure 16: Streamlines overlaid on velocity magnitude contours, indicating reduced flow recirculation in the vent passages.

3.3 Proposed Probe 3

Proposed Probe 3 (figure 17) used the characteristics from the literature review while fitting within the given manufacturing constraints; it is fully printable without any additional assembly. To achieve a more efficient design and comply with the diameter ratios from the literature, the outer diameter was slightly increased to 3.2 mm. Given the minimum printable thickness, this step helped in proposing a design similar to reference designs in the literature. In this design, the vents and the diffuser were designed similarly to Proposed Probe 2, which proved to be more aerodynamically efficient. Although this design met the requirement with the given constraints with a satisfying angular range, a drawback is the outer-to-inner diameter ratio of the inner probe due to the imposed thickness constraints.

CFD analysis showed an angular range of ±46°, still exceeding ±45°, however less than the previous probes. This suggests that the ratios of thickness and diameters of the inner probe and outer shield have a large impact on probe performance. Since this probe was practical to manufacture, it was chosen for printing and experimental testing.



(a) (b)

Figure 17: (a) Cross-sectional technical drawing of Proposed Probe 3 showing internal geometry. (b) 3D-printed fabricated probe used in experiments.

The experiment yielded results demonstrating probe efficiency beyond ±45°, reaching ±50.5°, greater than the Conventional Probe discussed earlier. Accordingly, the Conventional Probe and Proposed Probe 3 are compared based on the results from the experiments and simulations.

3.4 Results comparison: Proposed Probe 3 and Conventional Probe

Figures 18 and 19 present a comparative analysis of the experimental and CFD simulation results for both the Conventional Probe and Proposed Probe 3. The simulation findings of the Conventional Probe exhibit a difference of approximately 4° from the experimental findings on the positive side and 3° on the negative side (figure 18), which is within acceptable tolerance given common sources of numerical difference such as mesh resolution and solver limitations, experimental uncertainties, and manufacturing imperfections. To quantitatively assess probe performance and to follow the convention used by probe manufacturers [10], the pressure recovery factor (normalised total pressure) is used. It is defined as the ratio of the total pressure measured by the probe to the actual freestream total pressure, which in simulations is taken as the total pressure recorded at zero incidence angle:

$$\Pi_{\text{probe}} = \left| \frac{P_{\text{t}}^{\text{measured}}}{P_{\text{t}}^{\text{ref}}} \right| \tag{1}$$

In practical terms, a recovery factor of 1.00 ± 0.01 is commonly accepted as the threshold for 1% total pressure measurement error, serving as a benchmark for evaluating angular insensitivity performance. As illustrated by the plots, the angular insensitivity range of the pre-existing probe

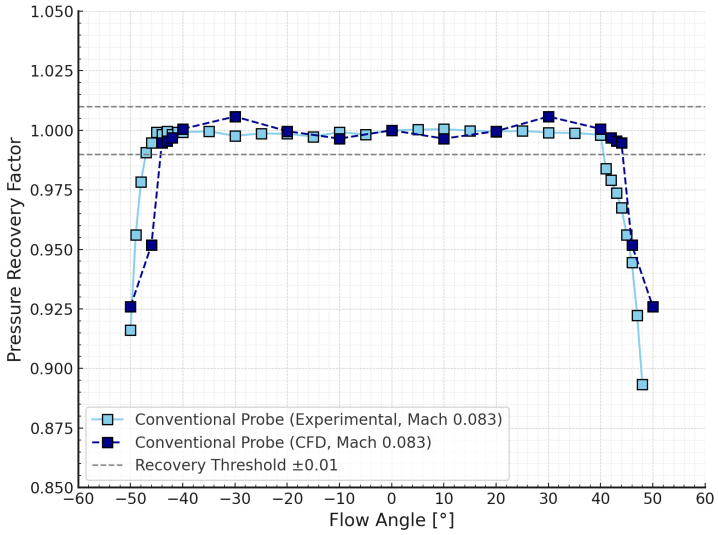


Figure 18: Pressure recovery factor with respect to flow angle for CFD and experimental data of the Conventional Probe.

is approximately 44° based on CFD results. From the experimental results, it is about 46° on the left side and 40° on the right side. Considering both experimental and simulation uncertainties, the experimental angular insensitivity range can be concluded as approximately 43° (average value), while the CFD results indicate about 44°. In contrast, Proposed Probe 3 demonstrates a significantly improved angular insensitivity range of around ±50.5° through experimental results after taking the averages from left and right sides (figure 19).

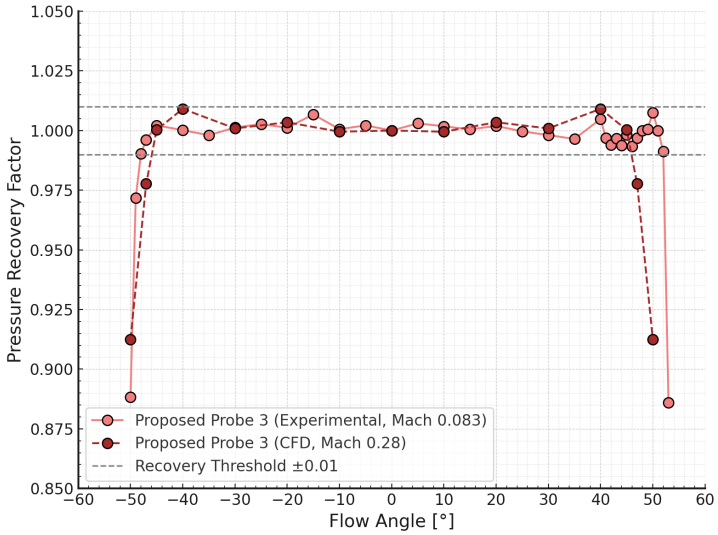


Figure 19: Pressure recovery factor with respect to flow angle for CFD and experimental data of Proposed Probe 3.

The discrepancy between the experimental and CFD results of Proposed Probe 3 can be attributed to several factors, including numerical errors, experimental uncertainty, manufacturing imperfections, and differences in Mach numbers. In the simulations, larger Mach numbers were used compared to the limited Mach range of the experimental facility, and literature supports

that, for shielded probes, as Mach number decreases, the angular insensitivity range increases [2].

The error values used to determine angular insensitivity are calculated using the formula:

$$\text{Total Pressure Error} = \left| \frac{P_t' - P_{t,\text{ref}}}{q_\infty} \right| \times 100 \tag{2}$$

where P_t' denotes the measured total pressure at incidence angle α, $P_{t,\text{ref}}$ is the reference total pressure at $\alpha = 0°$, and q_∞ is the freestream dynamic pressure. In the experiments (reported relative to ambient, i.e., gauge), $P_{t,\text{ref}} = P_t(\alpha = 0°) = q_\infty$.

The results (figure 20) show the comparison between the Conventional Probe and Proposed Probe 3 error values obtained from experimental results as they approach the angular insensitivity limit, defined as the angle at which the total pressure error reaches 1% [1, 2].

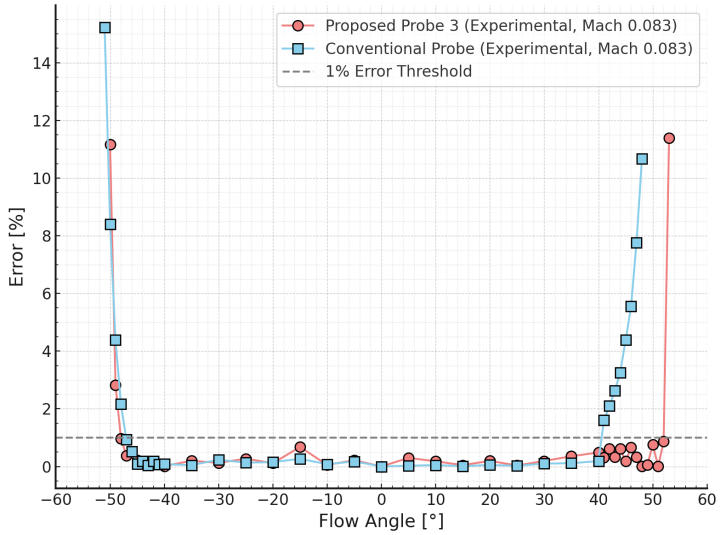


Figure 20: Error plot comparison between Conventional Probe and Proposed Probe 3 for experimental data.

3.5 Summary of results

The performance of Kiel-type shielded probes is governed by several geometric parameters discussed previously: the axial spacing ratio (a/D_1), the entrance angle (β), the vent-to-inlet area ratio (A_v/A_o), and two diameter ratios — the impact opening ratio (d/D) and the throat-to-shield ratio (D_2/D_1). These parameters are summarised for all four probe designs in table 2.

Literature supports that the axial spacing ratio (a/D_1) is most optimal at a value of 0.50 [1, 2], which is the value maintained in the proposed probes. In addition, since cylindrical inner probes have been used in this study, maximising the angular insensitivity range requires the impact opening diameter ratio (d/D) to be sufficiently large (close to 0.98) [2]. However, due to manufacturing constraints associated with the miniature size of the probe, the achieved ratios were smaller, with the smallest value occurring in Proposed Probe 3. This explains, in part, why the CFD results for Proposed Probe 3 show a reduced angular insensitivity range compared to the other probes. For the throat-to-shield ratio (D_2/D_1), the proposed probes adopted the standard ratio in order to comply with manufacturing limitations. Literature indicates that increasing the throat area can enhance the angular insensitivity range [2], which further explains

the reduced angular insensitivity range of Proposed Probe 3 relative to Proposed Probes 1 and 2. The entrance profiles of the proposed probes were chosen based on literature guidance to maximise angular insensitivity, using contoured entry surfaces rather than sharp tapers. Regarding vent geometry, the Conventional Probe and Proposed Probe 1 incorporated sharp elliptical and circular vent holes respectively, whereas Proposed Probes 2 and 3 employed optimised vents designed to promote smoother streamlines and reduce recirculation regions. Finally, although the vent-to-inlet area ratios (A_v/A_o) for the proposed probes were larger than the standard value of 1.5 (as in Proposed Probe 1), literature indicates that for ratios exceeding 1.5 the effect on angular insensitivity range becomes negligible [2].

Table 2: Comparison of key geometric parameters for all probes.

Parameter	**Conventional**	**Proposed 1**	**Proposed 2**	**Proposed 3**
Axial Spacing Ratio (a/D_1)	0.75	0.50	0.50	0.50
Impact Opening Ratio (d/D)	$<$0.698	0.698	0.698	$<$0.698
Throat-to-Shield Ratio (D_2/D_1)	0.67	0.50	0.50	0.50
Entrance Angle (β)	Smooth contoured	Smooth contoured	Smooth contoured	Smooth contoured
Vent Geometry	Elliptical	Circular	Optimised	Optimised
Vent-to-Inlet Area Ratio (A_v/A_o)	$>$1.5	1.5	$\gg$1.5	$\gg$1.5

The results of CFD and experimental investigations are summarised numerically in table 3.

Table 3: Summary of CFD and experimental performance results.

Metric	**Conventional**	**Proposed 1**	**Proposed 2**	**Proposed 3**
CFD Angular Insensitivity	$\pm 44°$	$\pm 53°$	$\pm 57°$	$\pm 46°$
Experimental Angular Insensitivity	$\pm 43°$	—	—	$\pm 50.5°$
Pressure Recovery (CFD)	1.00 ± 0.01 up to $\pm 44°$	1.00 ± 0.01 up to $\pm 53°$	1.00 ± 0.01 up to $\pm 57°$	1.00 ± 0.01 up to $\pm 46°$
Pressure Recovery (Exp.)	1.00 ± 0.01 up to $\pm 43°$	—	—	1.00 ± 0.01 up to $\pm 50.5°$

These tables consolidate the main findings of the study, showing how successive design iterations improved aerodynamic efficiency while meeting manufacturability constraints.

4 Conclusions

This study set out to develop and validate a compact Kiel-type probe, produced via additive manufacturing, that maintains reliable performance at high incidence angles. Of the discussed geometries, Proposed Probe 3 gave the best balance between performance and imposed geometric constraints, with an angular insensitivity range of approximately $\pm 50.5°$, considerably improved compared to the commercially available conventional design. This aerodynamic improvement is credited to its optimised vent geometry, enhanced diffuser design, and enhanced flow alignment in the shielded casing. The high-quality agreement between the experimental and simulated results supports the design, with the limited differences accounted for by typical experimental uncertainty and numerical discretisation behaviour. Despite miniaturised fabrication constraints, the obtained design achieves a good balance between manufacturability and aerodynamic performance. In comparison to the conventional probe, the new design had greater pressure recovery and less sensitivity to angle changes and was therefore a more reliable option.

Acknowledgments

The authors gratefully acknowledge the support of the Middle East Technical University Wind Energy Center (RÜZGEM) for providing access to the computational and experimental facilities employed in this study.

References

1. Kiel G 1935 *Total-head meter with small sensitivity to yaw* NACA Technical Memorandum 775 (National Advisory Committee for Aeronautics)

2. Gracey W 1956 *Wind-tunnel investigation of a number of total-pressure tubes at high angles of attack: Subsonic, transonic, and supersonic speeds* NACA Technical Note 3641 (National Advisory Committee for Aeronautics)

3. Russell W R, Gracey W, Letko W and Fournier P G 1951 *Wind-tunnel investigation of six shielded total-pressure tubes at high angles of attack: Subsonic speeds* NACA Technical Note 2530 (National Advisory Committee for Aeronautics)

4. Lejdeby A 2021 Design and calibration of pneumatic probes for aerodynamic testing *MSc Thesis* KTH Royal Institute of Technology, Stockholm

5. Gracey W, Pearson A O and Russell W R 1952 *Wind-tunnel investigation of a shielded total-pressure tube at transonic speeds* NACA Research Memorandum RM L51K19 (National Advisory Committee for Aeronautics)

6. PakTechPoint 2020 *Pitot tube design requirement in process industry* `https://paktechpoint.com/pitot-tube-design-requirement-pitot-tube-types/` (Accessed: 16 August 2025)

7. Mor-Yossef Y 2015 Separated flow prediction around a 6:1 prolate spheroid using Reynolds stress models *Differential Reynolds Stress Modeling for Separating Flows in Industrial Aerodynamics* ed B Eisfeld (Cham: Springer) pp 39–64

8. ANSYS Inc 2024 Section 4.11.2 Reynolds stress transport equations *ANSYS Fluent Theory Guide, Release 2024 R2* (Canonsburg, PA: ANSYS Inc)

9. Middle East Technical University 2025 *RÜZGEM (METUWIND) Centre for Wind Energy Research* `https://ruzgem.metu.edu.tr/en/` (Accessed: 23 January 2025)

10. Vectoflow 2025 *Kiel pressure probe datasheet* `https://vectoflow.com/wp-content/uploads/2024/03/2025-03-14_Vectoflow_Kiel-pressure-probe_Datasheet_EN.pdf` (Accessed: 14 March 2025)